CHIN. PHYS. LETT. Vol. 38, No. 2 (2021) 027401

Metal-Element-Incorporation Induced Superconducting Hydrogen Clathrate Structure at High Pressure

Jiayu Ma(马佳瑜)[1,2†], Junlin Kuang(匡均琳)[1†], Wenwen Cui(崔文文)[1*], Ju Chen(陈举)[1], Kun Gao(高琨)[1], Jian Hao(郝健)[1*], Jingming Shi(石景明)[1], and Yinwei Li(李印威)[1]

[1]*Laboratory of Quantum Functional Materials Design and Application, School of Physics and Electronic Engineering, Jiangsu Normal University, Xuzhou 221116, China*
[2]*CW Chu College, Jiangsu Normal University, Xuzhou 221116, China*

(Received 8 October 2020; accepted 2 December 2020; published online 27 January 2021)

The recent observation of high critical temperature T_c in lanthanum and Yttrium hydrides confirms the key role of hydrogen cage (H-cage) in determining high superconductivity. Here, we present a new class of metastable H_{12} clathrate structures based on the icosahedral $cI24$-Na that can be stabilized by incorporation of metal elements. Analysis shows that the charge transfer from metal atoms to H atoms contributes to forming the H_{12} clathrate. Nine dynamically stable structures are identified to exhibit superconductivity, and a maximum T_c of 28 K is found in voids-doped Mo_6H_{24}. Calculations reveal that the low T_c is attributed to the weak interaction between H atoms in each cage due to the long H–H distance. The current results provide a possible route to design H-cage containing superconductors.

DOI: 10.1088/0256-307X/38/2/027401

Hydrogen-rich materials are considered as promising high-T_c superconductors since they could be metallized at lower pressure due to the "chemical precompression effect" by the heavy elements as suggested by Ashcroft in 2004.[1] Subsequently, theoretical studies reveal vast numbers of hydrides with high-T_c under high pressure conditions,[2,3] among which H_3S[4] and LaH_{10}[5,6] have been experimentally confirmed and set record T_c values of ∼200 K and ∼260 K, respectively.

The superconductivity of hydrides is strongly dependent on the crystal structure and chemical bonding. Compounds containing hydrogen clathrate are considered as one of typical classes with high-T_c superconductivity under high pressure, e.g., CaH_6,[7] YH_6, YH_9, YH_{10},[8,9] LaH_{10},[10–16] MgH_6,[17] CeH_9,[18] PrH_9,[19,20] ThH_9, ThH_{10},[21,22] AcH_{10} and AcH_{16}.[23] In these hydrides, metal (M) atoms locate at the center of H-cages as electron donors, and the extra electrons elongate the bond length of H_2 molecules with the formation of weakly covalently bonded H-cages. Four types of H-cages have been reported: H_{24}-cages in MH_6, H_{29} or H_{28} in MH_9, H_{32} in MH_{10} and H_{40} in MH_{12}.[10,22] The predicted T_c values in all MH_6 (M = Ca, Y, Mg, etc.) exceed 200 K. For higher H content, the T_c's of YH_9, YH_{10},[8,9] LaH_{10},[10–15] AcH_{10} and AcH_{16},[23] are even up to 276 K (150 GPa), 303 K (400 GPa), 257–274 K (250 GPa), 204–251 K (200 GPa), and 199–241 K (150 GPa), respectively. Recently, a ternary hydride Li_2MgH_{16} with coexisted H_{18} and H_{28} cages was predicted to possess astonishing T_c of ∼470 K at 250 GPa,[24] which further confirms the potential of being high-T_c superconductors for clathrate structures.

An idea comes to mind naturally: are there alternative H-cages that could exist in hydrides? A previous theoretical study reported that Na transforms into a metallic icosahedral structure ($cI24$-Na) consisting of Na_{12} clathrate at terapamscal pressure.[25] Here, we examine the stability of H_{12} icosahedra constructed on basis of $cI24$-Na. Surprisingly, we find that the incorporation of metal elements in the cage center and/or in the cage voids could form several metastable compounds containing H_{12} cages. Interestingly, nine dynamically stable structures are identified with a maximum superconductivity of 28 K.

We choose $cI24$-Na (space group $Im\bar{3}$) as the parent structure and replace all the Na atoms with H atoms to construct H-cage structures [Fig. 1(a)]. There are two kinds of H–H distances in each H-cage, e.g., 0.78 and 0.87 Å at 3 TPa. Each H-cage contains 12H atoms, which consists of 12 isosceles triangles and 8 equilateral triangles. Nine H_{12} cages occupy the *bcc* lattice sites. We firstly examine the dynamical stability of pure H_{12}-cage structure by calculating phonon dispersions, and the occurrence of imaginary phonon frequencies in the first Brillouin zone indicates the dynamical instability in wide pressure ranges of 0–

Supported by the National Natural Science Foundation of China (Grant Nos. 12074154, 11722433, 11804128, 11804129, and 11904142), and the Qing Lan Project of Jiangsu Province.
†Jiayu Ma and Junlin Kuang contributed equally to this work.
*Corresponding authors. Email: wenwencui@jsnu.edu.cn; jian_hao@jsnu.edu.cn
© 2021 Chinese Physical Society and IOP Publishing Ltd

16 TPa. Then we attempt to stabilize H_{12} cage by doping metal elements in the cage center (A-site) or cage voids (B-site) (Fig. 1). We have tried at least 18 elements, including non-metallic metals (P, S, Se, B, Ar, As and Ge), the alkali metals (Li, Na and K) and the transition metals (Ta, Ti, Mo, W, Cr, Ba and Hf), following four doping types as: (1) A-site only; (2) B-site only; (3) A-, B-sites with same atoms; (4) A-, B-sites with different atoms. We found that in case 3, all considered structures are dynamically unstable; in case 1, the considered structures are either dynamically unstable or the H_{12} cages collapse after optimization. Surprisingly, we have successfully found 3 binary and 6 ternary dynamically stable compounds in cases 2 and 4, respectively [see Figs. 1(b) and 1(c)] with negative formation enthalpies respective to element atoms (Table S1). Note that the space group for nice structures evolves to $Im\bar{3}m$ and H–H distance was significantly elongated (Table S5) due to the metal incorporation. Interestingly, all nine compounds exhibit superconductivity [Fig. 1(c)], among which Mo_6H_{24} (T_c = 28 K) and $Ti_6Na_2H_{24}$(T_c = 3.92 K) possess the highest T_c in the stable binary and ternary compounds, respectively. Therefore, we focus on these two compounds in following analysis and discussions.

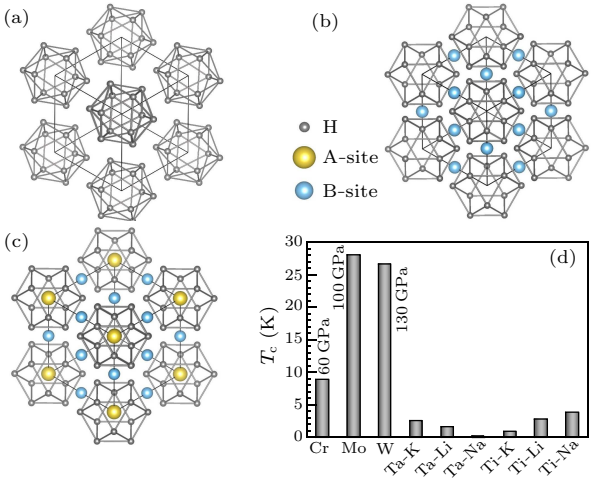

Fig. 1. The clathrate structures and superconductivity derivative from *cI*24-Na. (a)–(c) The structures of pure H-clathrate H_{24}, B_2H_{24}, and $A_6B_2H_{24}$, respectively. (d) The calculated T_c for nine dynamically stable systems.

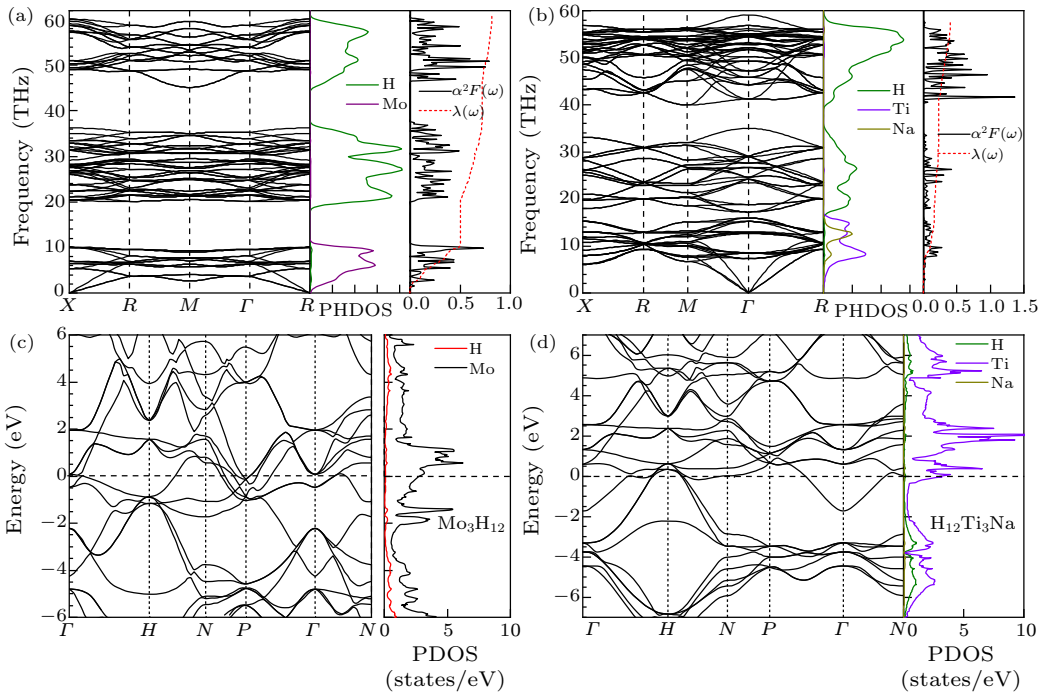

Fig. 2. (a) and (b) Phonon spectra, projected phonon density of states (PHDOS), Eliashberg spectral function [$\alpha^2F(\omega)$], and $\lambda(\omega)$ of Mo_6H_{24} and $Ti_6Na_2H_{24}$ at 100 GPa, respectively. (c) and (d) Band structures and projected DOS of Mo_6H_{24} and $Ti_6Na_2H_{24}$ at 100 GPa, respectively.

Analysis of atoms in molecules reveals that there are 0.24e transferred from Mo to H in Mo_6H_{24} at 100 GPa (Table 1). Same electrons are added to H in $Ti_6Na_2H_{24}$, in which 0.19e and 0.05e are from Ti and Na, respectively. The additional electrons donated from metal atoms occupy the antibonding σ^*, resulting in the elongation of the H–H distance. For instance, the distances of H–H in Mo_6H_{24} and $Ti_6Na_2H_{24}$ at 100 GPa are 1.65 Å and 1.85 Å, respectively. The current results indicate that the metal atoms are electron donors and help to stabilize the H-cage at high pressures.

Phonon dispersions are calculated to verify the dynamical stability of the candidate structures. As shown in Figs. 2(a) and 2(b), the absence of imaginary frequencies of the calculated phonon dispersions

at 100 GPa for Mo_6H_{24} and $Ti_6Na_2H_{24}$ indicate their dynamical stability. Surprisingly, we find that the incorporation of metal elements could stabilize the H_{12} cages from ambient pressure up to 100 GPa in Mo_6H_{24}. The frequencies initiatively separate into three parts: the vibration mode of the H atoms mainly dominates the vibrational states in the high and medium frequency regions (>10 THz), while the heavy atoms contribute to the low frequency regions (<10 THz). Additionally, compared to the ternary $Ti_6Na_2H_{24}$ system, it exhibits a more distinct hierarchy in the binary Mo_6H_{24} systems. With increasing pressures, the frequencies of H atoms begin to play an important role and favor to form a clear hierarchy as compared to the phonons of Mo_6H_{24} at 0 GPa (Fig. S1e).

Table 1. Bader chargers of Mo_6H_{24} and $Ti_6Na_2H_{24}$ at 100 GPa. A negative (positive) sign indicates an electron gain (loss) for the particular atom.

Compounds	Pressures (GPa)	Atoms	Charge (e)
Mo_6H_{24}	100	Mo	0.96
		H	−0.24
$Ti_6Na_2H_{24}$	100	Ti	0.78
		Na	0.60
		H	−0.24

The band structures and densities of states (DOSs) are calculated to obtain the electronic properties. Figures 2(c) and 2(d) indicate that both Mo_6H_{24} and $Ti_6Na_2H_{24}$ exhibit metallic features with several bands crossing the Fermi level E_F. However, the binary and ternary compounds exhibit the similar feature in which the DOSs around E_F are nearly formed by the metal atoms rather than H atoms. Moreover, in the ternary $Ti_6Na_2H_{24}$, Ti dominates the DOS at the E_F instead of Na due to its one valence electron. Note that the feature of metal-element-dominated DOS at E_F can also be found in other 7 dynamically stable compounds (see Fig. S1).

In order to investigate the bonding behavior of the structures, we calculate the electron localization function.[26] From Figs. 3(a) and 3(b) in [111] plane, it is evident that the electrons gather and pervade around the H atoms. Further, there is no evidence for the existence of the covalent bonding between the H atoms, different from the weak covalent interaction between H atoms in the previously proposed superconducting clathrate hydrides.[7–9] This also explains why the structures cannot possess high good superconductivity. Two ways can promote the formation of weak H–H covalent bonding: (i) High pressure can shorten the length of the H–H bond, however, it is out of the stability range for our candidate structures. (ii) Cages with more H atoms can be constructed to share the donated electrons of metals, resulting in short H–H distance. The T_c's in all the stable compounds are estimated by the Allen–Dynes modified McMillan formula,[27] as shown in Fig. 1(c). The calculated T_c's of the structures show a striking contrast on the binary and ternary system. Mo_6H_{24} possesses the highest T_c around 28 K at 100 GPa in the binary compounds, while $Ti_6Na_2H_{24}$ exhibits the highest T_c (around 3.93 K at 100 GPa) in the ternary compounds. In fact, the calculated electron-phonon coupling (EPC) parameter λ (0.84) in Mo_6H_{24} is triple of that in $Ti_6Na_2H_{24}$ (0.27) at the same pressure (100 GPa), therefore leading to a higher T_c value [Figs. 2(a) and 2(b)]. The contribution from the metal Mo (<11 THz) to the λ (65%) is larger than that of H atoms (35%), which is different from CaH_6, wherein the H atoms contribute 81% to the total λ of 2.69.[7] The EPC parameter λ of the other seven compounds are listed in Table S7 and the corresponding T_c's are calculated as follows: W_6H_{24} (26.6 K), Cr_6H_{24} (8.95 K), $Ta_6K_2H_{24}$ (2.56 K), $Ta_6Li_2H_{24}$ (1.6 K), $Ta_6Na_2H_{24}$ (0.12 K), $Ti_6K_2H_{24}$ (0.91 K) and $Ti_6Li_2H_{24}$ (2.94 K). The small EPC (0.27–0.98) is also due to the relatively small H-derived DOS contribution at Fermi level. Note that all the estimated T_c values are much lower than that of reported cage structures with T_c's larger than 200 K (YH_6,[8,9] CaH_6,[7] YH_{10},[8,9] LaH_{10},[10–15] MgH_6,[17] etc.), among which YH_6 and LaH_{10} have been successfully synthesized and measured with T_c of 224 K at 166 GPa[9] and 250–260 K above 150 GPa,[5,6] respectively. When comparing with the distances of these structures, we find that the H–H lengths in these clathrates range from 1.1 Å to 1.31 Å, which is much shorter than those of our structures (1.65–1.85 Å), indicating the necessity to construct H-cages with shorter H–H distance and more H atoms in the further study.

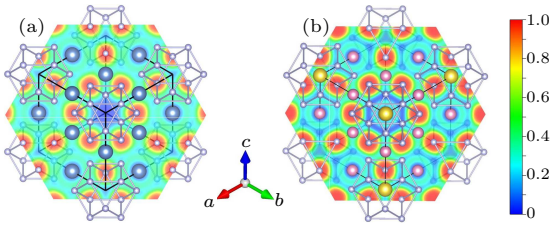

Fig. 3. The ELF of (a) Mo_6H_{24} and (b) $Ti_6Na_2H_{24}$ at 100 GPa, respectively.

In conclusion, we have identified nine dynamically stable superconductors deriving from $cI24$-Na structures. Compared to the ternary compounds, the binary interstitial-structures tend to show a higher T_c because of the shorter H–H distance. However, the low content (∼75% and 80%) of H atoms in the small cages limits the formation of weaker H–H covalent bonding, which is responsible for the higher T_c in structures of clathrate hydrides. We successfully provide a route to construct the dynamically stable H-clathrate structures. Our results indicate that exploration of H-clathrate structures with more H atoms and shorter

H–H distance may be a possible route to approaching higher-T_c superconductors.

Methods.—Based on the density function theory, the structure optimization and the electron structure calculation are performed in the Vienna *ab initio* simulation package (VASP)[28] in the projector augmented-wave method.[29] The exchange-correlation function is the generalized gradient approximation theory of Perdew, Burke and Ernzerhof.[30] The cutoff energy of the wave function into the plane wave basis is settled with 1000 eV. The large-scale elements research by estimating the dynamic stability of the doping structure is implemented in the VASP through PHONOPY, which is an open source package for phonon calculations at harmonic and quasi-harmonic levels. Among the dynamical calculations, a q-mesh of $20 \times 20 \times 20$ is adopted for phonon calculations. The Monkhorst–Pack k-point meshes with a grid density of $0.20\,\text{Å}^{-1}$ are chosen to ensure that the total energy convergence is better than 1 meV per atom and the kinetic energy cutoff is settled as 1000 eV. The valence electrons for the investigated 18 elements are listed in Table S8. The phonon spectrums redacted in the text and the electron-phonon coupling (EPC) are computed in the QUANTUM ESPRESSO code (QE)[31] using the density-functional perturbation theory. Among all the QE calculations, a q-mesh of $6 \times 6 \times 6$ and a k-mesh of $12 \times 12 \times 12$ for the $Im\bar{3}m$ phase are adopted to ensure convergence in the first Brillouin zone. The value of gaussian spreading for Brillouin zone is 0.04 Ry through the calculation of EPC parameter λ and the Eliashberg spectral function $\alpha^2F(\omega)$.

All the calculations were performed at the High Performance Computing Center of the School of Physics and Electronic Engineering of Jiangsu Normal University.

References

[1] Ashcroft N W 2004 *Phys. Rev. Lett.* **92** 187002
[2] Cui W and Li Y 2019 *Chin. Phys. B* **28** 107104
[3] Zhang L, Wang Y, Lv J and Ma Y 2017 *Nat. Rev. Mater.* **2** 17005
[4] Drozdov A, Eremets M, Troyan I, Ksenofontov V and Shylin S 2015 *Nature* **525** 73
[5] Drozdov A P, Kong P P, Minkov V S, Besedin S P, Kuzovnikov M A, Mozaffari S, Balicas L, Balakirev F F, Graf D E, Prakapenka V B, Greenberg E, Knyazev D A, Tkacz M and Eremets M I 2019 *Nature* **569** 528
[6] Somayazulu M, Ahart M, Mishra A K, Geballe Z M, Baldini M, Meng Y, Struzhkin V V and Hemley R J 2019 *Phys. Rev. Lett.* **122** 27001
[7] Wang H, Tse J, Tanaka K, Iitaka T and ma Y 2012 *Proc. Natl. Acad. Sci. USA* **109** 6463
[8] Li Y, Hao J, Liu H, Tse J, Wang Y and Ma Y 2015 *Sci. Rep.* **5** 9948
[9] Troyan I, Semenok D, Kvashnin A, Ivanova A, Prakapenka V, Greenberg E, Gavriliuk A, Lyubutin I, Struzhkin V and Oganov A 2019 arXiv:1908.01534 [cond-mat.supr-con]
[10] Peng F, Sun Y, Pickard C J, Needs R J, Wu Q and Ma Y 2017 *Phys. Rev. Lett.* **119** 107001
[11] Liu H Y, Naumov I I, Hoffmann R, Ashcroft N W and Hemley R J 2017 *Proc. Natl. Acad. Sci. USA* **114** 6990
[12] Papaconstantopoulos D A, Mehl M J and Chang P H 2020 *Phys. Rev. B* **101** 060506
[13] Durajski A P, Szczesniak R, Li Y, Chongze W J H C, Wang C and Cho J H 2020 *Phys. Rev. B* **101** 214501
[14] Elatresh S F, Timusk T and Nicol E J 2020 *Phys. Rev. B* **102** 024501
[15] Kostrzewa M, Szczęśniak K M, Durajski A P and Szczęśniak R 2020 *Sci. Rep.* **10** 1
[16] Errea I, Belli F, Monacelli L, Sanna A, Koretsune T, Tadano T, Bianco R, Calandra M, Arita R, Mauri F and Flores-Livas J A 2020 *Nature* **578** 66
[17] Feng X L, Zhang J R, Gao G Y, Liu H Y and Wang H 2015 *RSC Adv.* **5** 59292
[18] Salke N P, Davari E M M, Zhang Y, Kruglov I A, Zhou J, Wang Y, Greenberg E, Prakapenka V B, Liu J, Oganov A R and Lin J F 2019 *Nat. Commun.* **10** 1
[19] Peña-Alvarez M, Binns J, Hermann A, Kelsall L C, Dalladay-Simpson P, Gregoryanz E and Howie R T 2019 *Phys. Rev. B* **100** 184109
[20] Zhou D, Semenok D V, Duan D, Xie H, Chen W, Huang X, Li X, Liu B, Oganov A R and Cui T 2020 *Sci. Adv.* **6** eaax6849
[21] Kvashnin A G, Semenok D V, Kruglov I A, Wrona I A and Oganov A R 2018 *ACS Appl. Mater. & Interfaces* **10** 43809
[22] Semenok D V, Kvashnin A G, Ivanova A G, Svitlyk V, Fominski V Y, Sadakov A V, Sobolevskiy O A, Pudalov V M, Troyan I A and Oganov A R 2020 *Mater. Today* **33** 36
[23] Semenok D V, Kvashnin A G, Kruglov I A and Oganov A R 2018 *J. Phys. Chem. Lett.* **9** 1920
[24] Sun Y, Lv J, Xie Y, Liu H and Ma Y 2019 *Phys. Rev. Lett.* **123** 97001
[25] Li Y, Wang Y, Pickard C J, Needs R J, Wang Y and Ma Y 2015 *Phys. Rev. Lett.* **114** 125501
[26] Becke A D and Edgecombe K E 1990 *J. Chem. Phys.* **92** 5397
[27] Allen P B and Dynes R C 1975 *Phys. Rev. B* **12** 905
[28] Kresse G and Furthmüller J 1996 *Phys. Rev. B* **54** 11169
[29] Kresse G and Joubert D 1999 *Phys. Rev. B* **59** 1758
[30] Perdew J P, Burke K and Ernzerhof M 1996 *Phys. Rev. Lett.* **77** 3865
[31] Giannozzi P, Baroni S, Bonini N, Calandra M, Car R, Cavazzoni C, Ceresoli D, Chiarotti G L, Cococcioni M, Dabo I, Corso A D, de Gironcoli S, Fabris S, Fratesi G, Gebauer R, Gerstmann U, Gougoussis C, Kokalj A, Lazzeri M, Martin-Samos L, Marzari N, Mauri F, Mazzarello R, Paolini S, Pasquarello A, Paulatto L, Sbraccia C, Scandolo S, Sclauzero G, Seitsonen A P, Smogunov A, Umari P and Wentzcovitch R M 2009 *J. Phys.: Condens. Matter* **21** 395502

Supplementary information for "Metal-element-incorporation induced superconducting hydrogen clathrate structure at high pressure"

Jiayu Ma(马佳瑜)[1,2#], Junlin Kuang(匡均琳)[1#], Wenwen Cui(崔文文)[1]*, Ju Chen(陈举)[1], Kun Gao(高琨)[1], Jian Hao(郝健)[1]*, Jingming Shi(石景明)[1] and Yinwei Li(李印威)[1]

Laboratory of Quantum Functional Materials Design and Application, School of Physics and Electronic Engineering, Jiangsu Normal University, Xuzhou 221116, China

wenwencui@jsnu.edu.cn; jiao_hao@jsnu.edu.cn

Table S1. All of the ternary systems we tried and the external pressure we presumed. Atom A and B are referred to FIG.1.

Ternary System	Position		Pressure	Stability
	Atom A	Atom B	（GPa）	
$Ta_6Li_2H_{24}$	Ta	Li	70-190	√
$Ta_6Na_2H_{24}$	Ta	Na	25-350	√
$Ta_6K_2H_{24}$	Ta	K	60-200	√
$Ti_6Li_2H_{24}$	Ti	Li	100-200	√
$Ti_6Na_2H_{24}$	Ti	Na	100-250	√
$Ti_6K_2H_{24}$	Ti	K	100-150	√
$P_6S_2H_{24}$	P	S	50-200	×
$S_6Na_2H_{24}$	S	Na	100-200	×
$Se_6Na_2H_{24}$	Se	Na	200	×
$Na_6Se_2H_{24}$	Na	Se	50-150	×
$Mo_6Se_2H_{24}$	Mo	Se	50-200	×
$W_6Se_2H_{24}$	W	Se	50	×
$S_6Se_2H_{24}$	S	Se	50	×
$Se_6B_2H_{24}$	Se	B	50-300	×

Table S2. All of the binary systems we tried and the external pressure we presumed. Atom A and B are referred to FIG.1.

Binary System	Position		Pressure	Stability
	Atom A	Atom B	(GPa)	
Cr_6H_{24}	Cr	--	30-60	√
As_6H_{24}	As	--	100-400	×
Mo_6H_{24}	Mo	--	0-100	√
Ba_6H_{24}	Ba	--	100-500	×
Hf_6H_{24}	Hf	--	50-200	×
W_6H_{24}	W	--	85-130	√
Bi_6H_{24}	Bi	--	100-300	×
S_2H_{24}	--	S	50-200	×
Ar_2H_{24}	-	Ar	50-300	×
Ge_2H_{24}	--	Ge	100-300	×
As_2H_{24}	--	As	50-500	×
Se_2H_{24}	--	Se	55-65	√
Te_2H_{24}	--	Te	50-150	×
Ba_2H_{24}	--	Ba	300	×

Table S3 The formation enthalpies ΔH (eV/atom) of dynamically stable compounds relative to element atoms.

		ΔH
Binary system	Cr_6H_{24} (60GPa)	-0.070
	W_6H_{24} (100GPa)	-0.050
	Mo_6H_{24} (100GPa)	0.046
Ternary system (100 GPa)	$Ta_6Li_2H_{24}$	-0.520
	$Ta_6Na_2H_{24}$	-0.516
	$Ta_6K_2H_{24}$	-0.369
	$Ti_6Li_2H_{24}$	-0.802
	$Ti_6Na_2H_{24}$	-0.778
	$Ti_6K_2H_{24}$	-0.608

Table S4. Detailed structure information of our stable ternary systems after optimization.

Ternary System (100GPa)	a (=b=c)	H Atoms	Atom A	Atom B	Volume ($Å^3$)
$Ta_6Li_2H_{24}$	5.2349	24h(0,0.242,0.242)	6b(0.5,0,0)	2a(0.5,0.5,0.5)	143.458
$Ta_6Na_2H_{24}$	5.3192	24h(0.250,0,-0.250)	6b(1,0.5,0)	2a(0.5,0.5,0.5)	150.500
$Ta_6K_2H_{24}$	5.4158	24h(0,0.259,0.259)	6b(0.5,0,0)	2a(0.5,0.5,0.5)	158.850
$Ti_6Li_2H_{24}$	5.722	24h(0,0.260,0.260)	6b(0.5,0,0)	2a(0.5,0.5,0.5)	187.346
$Ti_6Na_2H_{24}$	5.0979	24h(0,0.257,0.257)	6b(0.5,0,0)	2a(0.5,0.5,0.5)	132.487
$Ti_6K_2H_{24}$	5.2069	24h(0,0.266,0.266)	6b(0.5,0,0)	2a(0.5,0.5,0.5)	141.168

Table S5. Detailed structure information of our stable binary systems after optimization.

Binary System	Pressure	a (=b=c)	H Atoms	Atom A	Atom B	Volume ($Å^3$)
Cr_6H_{24}	30Gpa	5.0125	24h(0,0.245,0.245)	6b(0,0.5,0)	-	125.940
	60Gpa	4.8536	24h(0,0.240,0.240)	6b(0,0.5,0)	-	114.338
Mo_6H_{24}	0Gpa	5.6593	24h(0,0.254,0.254)	6b(0,0.5,0)	-	181.254
	100Gpa	5.0415	24h(0,0.231,0.231)	6b(0,0.5,0)	-	128.138
W_6H_{24}	95Gpa	5.1163	24h(0,0.231,0.231)	6b(0,0.5,0)	-	133.927
	130Gpa	5.0041	24h(0,0.226,0.225)	6b(0,0.5,0)	-	125.308
Se_2H_{24}	60Gpa	4.4765	24g(0,0.408,0.186)	-	2a(0,0,0)	89.705

Table S6. The H-H distance in the abstract clathrate of FIG. 1(a) and (b). The suffix represents the external pressure.

ternary system -100GPa	H-H distance (Å)	binary system -pressure	H-H distance (Å)
$Ta_6Li_2H_{24}$	1.79	Cr_6H_{24}-30 GPa	1.74
$Ta_6Na_2H_{24}$	1.88	Cr_6H_{24}-60 GPa	1.65
$Ta_6K_2H_{24}$	1.99	Mo_6H_{24}-0 GPa	2.03
$Ti_6Li_2H_{24}$	2.11	Mo_6H_{24}-100 GPa	1.65
$Ti_6Na_2H_{24}$	1.85	W_6 H_{24}-95 GPa	1.67
$Ti_6K_2H_{24}$	1.96	W_6H_{24}-130 GPa	1.60

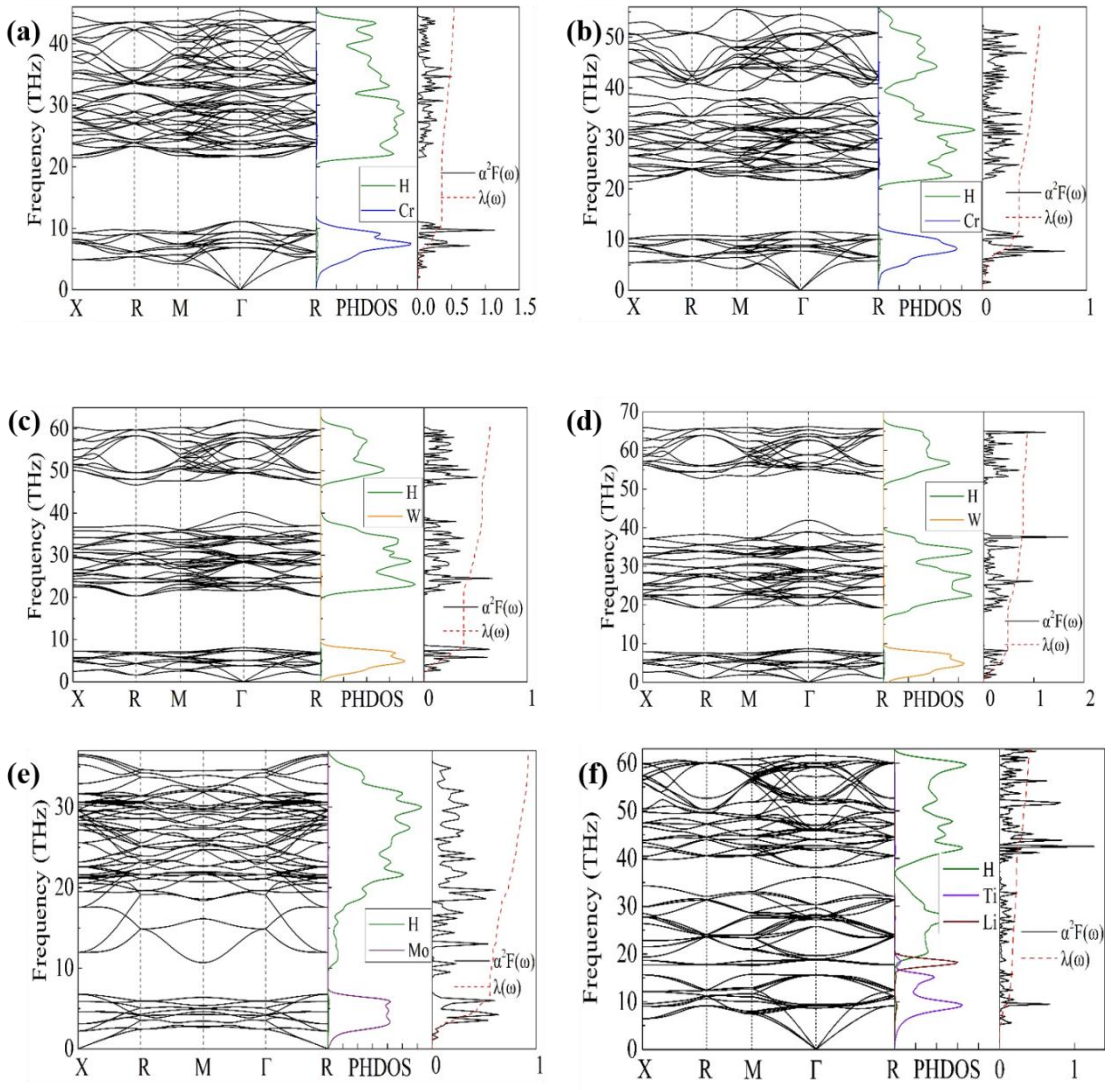
(a)
(b)
(c)
(d)
(e)
(f)
Frequency (THz)
X R M Γ R PHDOS
H
Cr
W
Mo
Ti
Li
α²F(ω)
λ(ω)

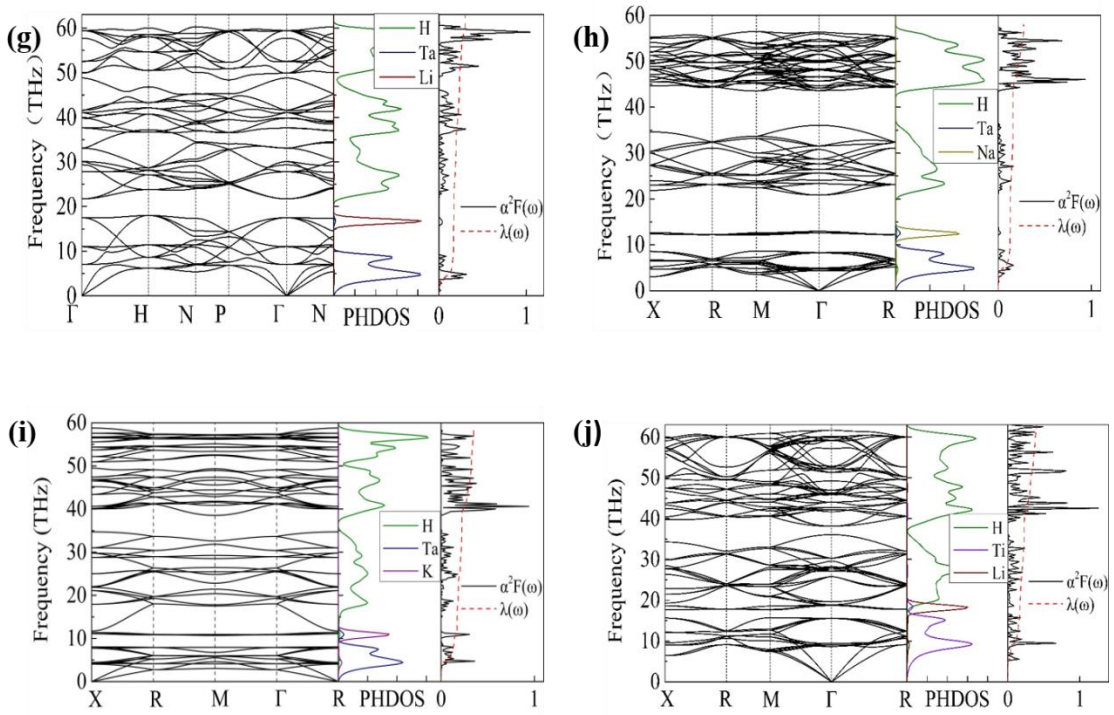

Figure S1. Computed phonon spectra of Cr_6H_{24} at 30GPa (a), Cr_6H_{24} at 60GPa (b), W_6H_{24} at 95GPa (c), W_6H_{24} at 130GPa (d), Mo_6H_{24} at 0GPa (e), $Ti_6Li_2H_{24}$ (f), $Ta_6Li_2H_{24}$ (g), $Ta_6Na_2H_{24}$ h), $Ta_6K_2H_{24}$ (i), $Ti_6Li_2H_{24}$ (j), all of the $A_6B_2H_{24}$ are 100GPa. Showing the dynamical stabilities of these phases.

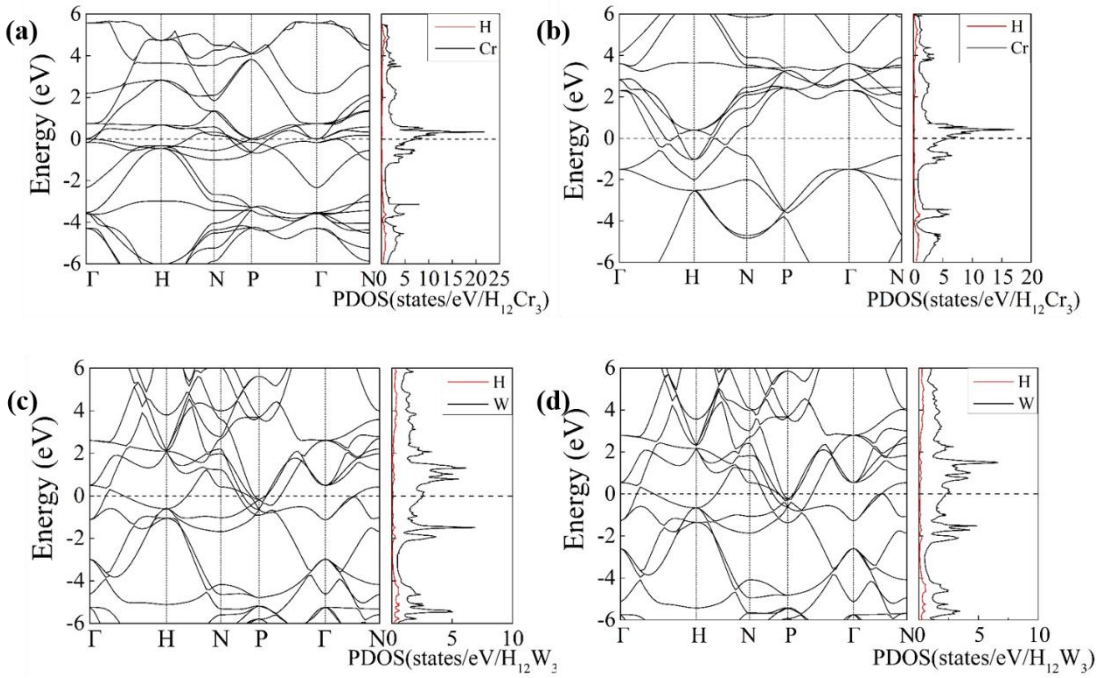

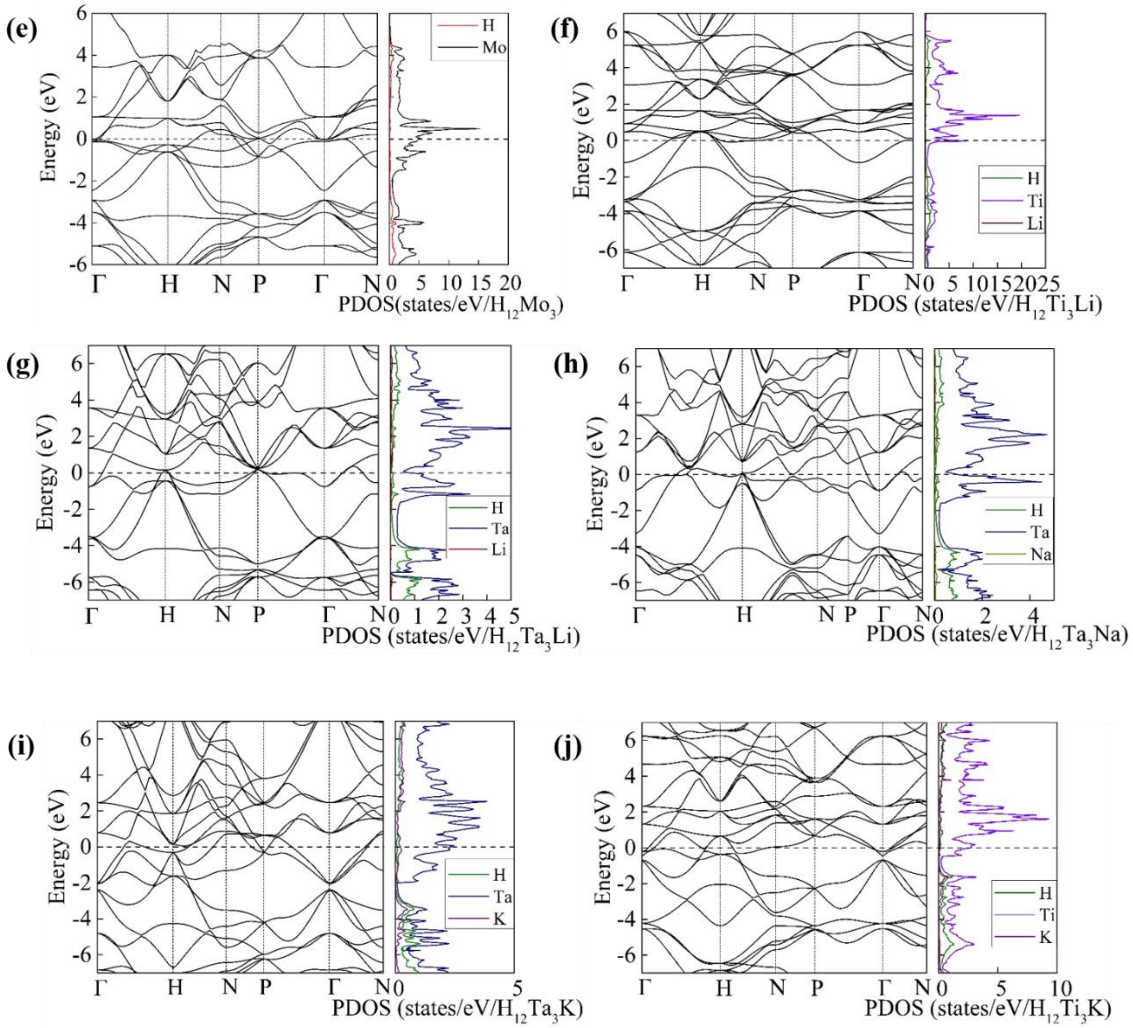

Fig S2. The band structure and the electron density of states for Cr_6H_{24} at 30GPa (a), Cr_6H_{24} at 60GPa (b), W_6H_{24} at 95GPa (c), W_6H_{24} at 130GPa (d), Mo_6H_{24} at 0GPa (e), $Ti_6Li_2H_{24}$ (f), $Ta_6Li_2H_{24}$ (g), $Ta_6Na_2H_{24}$ h), $Ta_6K_2H_{24}$ (i), $Ti_6K_2H_{24}$ (j), all of the $A_6B_2H_{24}$ are 100GPa. Showing the metallic features of these phases.

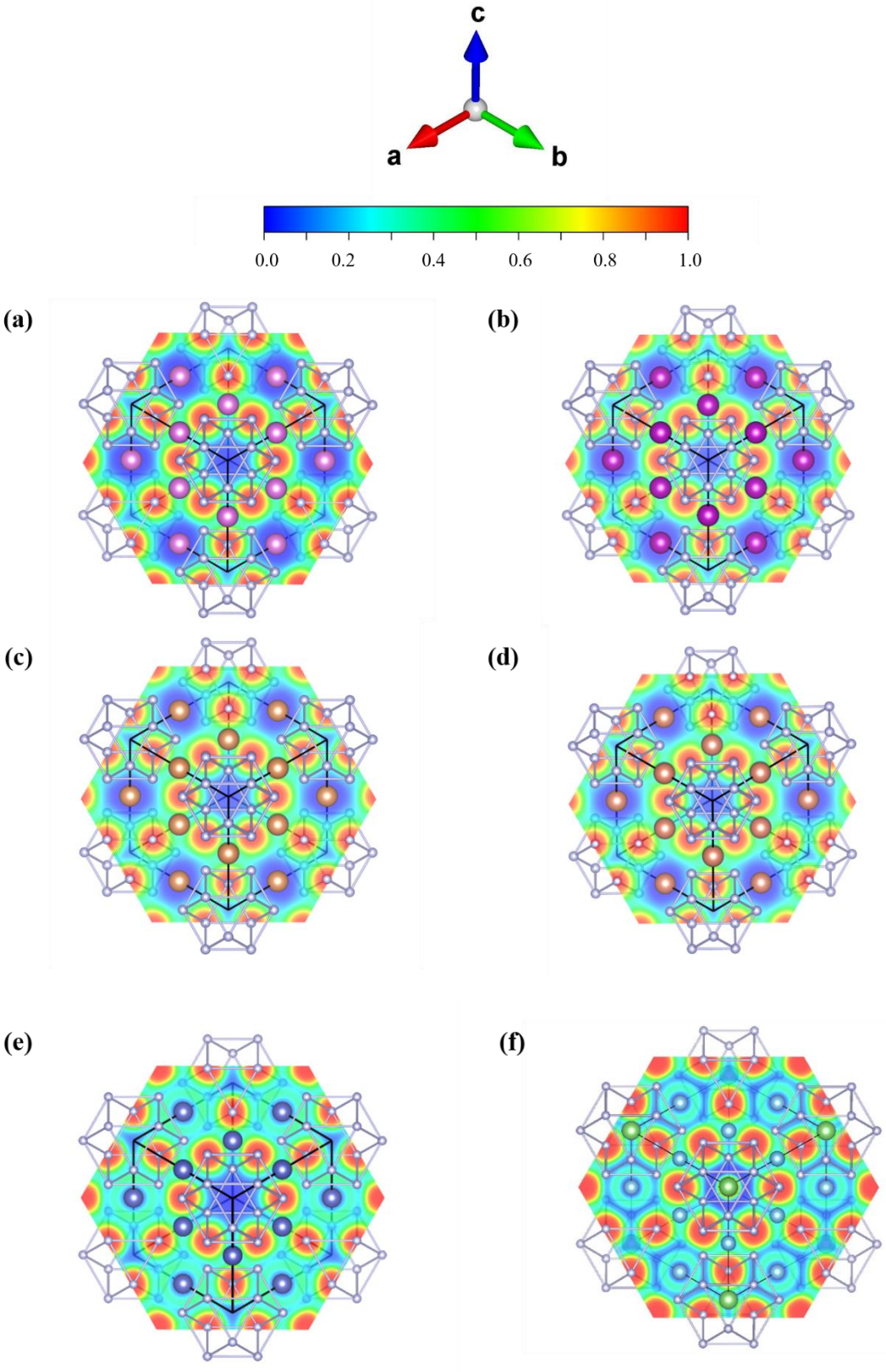
c
a
b
0.0
0.2
0.4
0.6
0.8
1.0
(a)
(b)
(c)
(d)
(e)
(f)

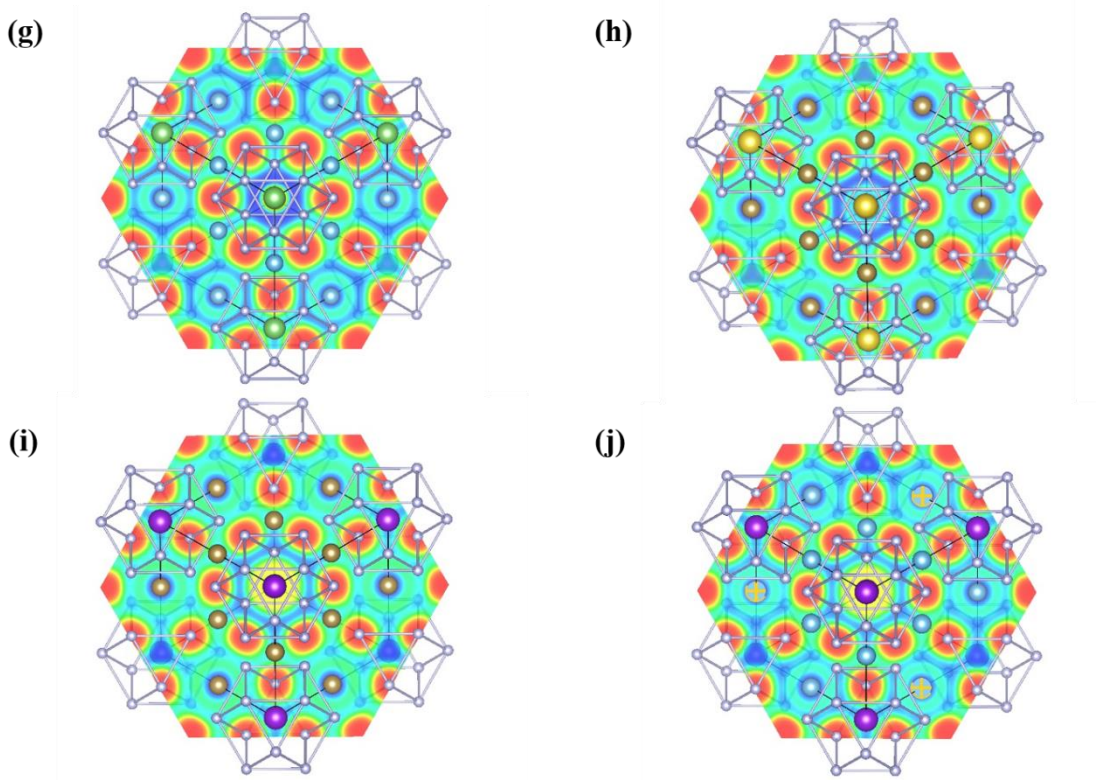

Fig S3. The ELF graph of Cr_6H_{24} at 30GPa (a), Cr_6H_{24} at 60GPa (b), W_6H_{24} at 95GPa (c), W_6H_{24} at 130GPa (d), Mo_6H_{24} at 0GPa (e), $Ti_6Li_2H_{24}$ (f), $Ta_6Li_2H_{24}$ (g), $Ta_6Na_2H_{24}$ (h), $Ta_6K_2H_{24}$ (i), $Ti_6K_2H_{24}$ (j), all of the $A_6B_2H_{24}$ are 100GPa.

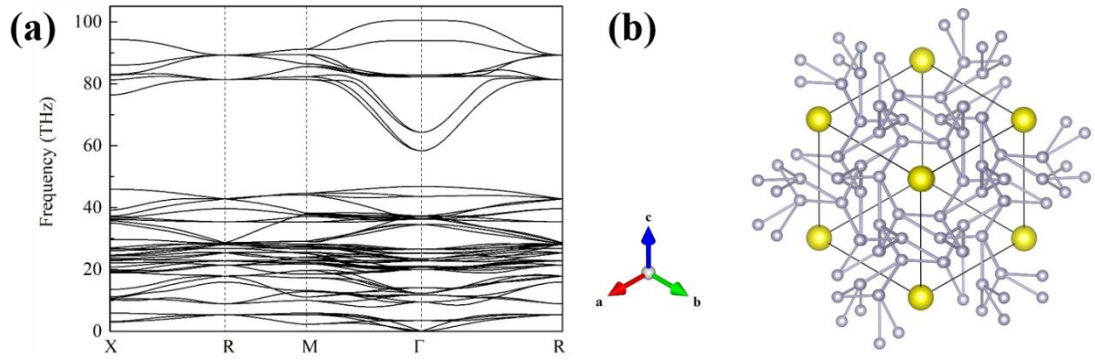

Fig S4. The phonon graph of stable system Se_2H_{24} at 60Gpa (a), the space group of the structure is *Im-3m*. Unfortunately, the structure of H-clathrate lose (b).

Table S7. The calculated electron-phonon parameters λ, the Logarithmic Average Phonon Frequency ω_{log} and Electronic Density of states at the Fermi level **N (ε_f)** of our stable systems. The pressure of our Ternary systems are all 100 GPa.

		T_c (K)	**λ**	**ω_{log} (K)**	**N (ε_f)**
Binary system	Cr_6H_{24} (30GPa)	8.56	0.53	574.96	49.57
	Cr_6H_{24} (60GPa)	8.95	0.53	583.59	40.25
	W_6H_{24} (95GPa)	14.6	0.64	541.15	18.82
	W_6H_{24} (130GPa)	16.6	0.87	485.36	17.03
	Mo_6H_{24} (0GPa)	24.4	0.98	363.47	38.09
	Mo_6H_{24} (100GPa)	28.0	0.84	545.54	21.58
Ternary system	$Ta_6Li_2H_{24}$	1.63	0.37	578.36	11.88
	$Ta_6Na_2H_{24}$	0.12	0.27	771.58	14.53
	$Ta_6K_2H_{24}$	2.59	0.39	743.09	20.07
	$Ti_6Li_2H_{24}$	2.94	0.37	1029.50	18.33
	$Ti_6Na_2H_{24}$	3.92	0.39	1059.69	20.95
	$Ti_6K_2H_{24}$	0.91	0.33	869.32	15.29

Table S8. Valence configuration for VASP POTCARs used for our investigated elements

Element	PBE-PAW File Name	Valence Configuration
H	H_h	$1s^1$
Ta	Ta_pv	$5p^6 6s^2 5d^3$
Li	Li_sv	$1s^1 2s^1 2p^1$
Na	Na_pv	$2p^6 3s^1$
K	K_sv	$3s^2 3p^6 4s^1$
Ti	Ti_pv	$3d^3 4s^1$
Mo	Mo_pv	$4p^6 5s^1 4d^5$
W	W	$6s^2 5d^4$
Hf	Hf	$6s^1 5d^2$
Ba	Ba_sv	$5s^2 5p^6 6s^2$
Cr	Cr	$3d^5 4s^1$
S	S	$3s^2 3p^4$
Se	Se	$4s^2 4p^4$
As	As	$4s^2 4p^3$
Ge	Ge	$4s^2 4p^2$
Ar	Ar	$3s^2 3p^6$
B	B	$2s^2 2p^1$
P	P	$3s^2 3p^3$